CONFIDENTIAL

Copy
RM L55F22a

RESEARCH MEMORANDUM

INVESTIGATION AT TRANSONIC SPEEDS OF AERODYNAMIC CHARACTERISTICS OF AN UNSWEPT SEMIELLIPTICAL AIR INLET IN THE ROOT OF A 45° SWEPTBACK WING

By Gene J. Bingham

Langley Aeronautical Laboratory
Langley Field, Va.

CLASSIFIED DOCUMENT

NATIONAL ADVISORY COMMITTEE
FOR AERONAUTICS

WASHINGTON
September 28, 1955

CONFIDENTIAL

NATIONAL ADVISORY COMMITTEE FOR AERONAUTICS

RESEARCH MEMORANDUM

INVESTIGATION AT TRANSONIC SPEEDS OF AERODYNAMIC CHARACTERISTICS OF AN UNSWEPT SEMIELLIPTICAL AIR INLET IN THE ROOT OF A 45° SWEPTBACK WING

By Gene J. Bingham

SUMMARY

An investigation has been made in the Langley transonic blowdown tunnel at Mach numbers from 0.65 to 1.40 to study the internal and external aerodynamic characteristics of an unswept semielliptical air intake installed in the root of a 45° sweptback wing. Tests were made over an angle-of-attack range from 0° to 9.6° at mass-flow ratios from about 0.55 to 0.90. The results of this investigation have been compared with those of a similar inlet swept back along the wing leading edge.

Increases in compressor-face total-pressure recovery $\bar{H}/H_o$ with decreasing inlet mass-flow ratio were effected at all test conditions. This trend was attributed to a "natural" bypassing of a large part of the boundary-layer flow around the lower inlet lip which was staggered 30°. The bypassing was more complete at the low mass-flow ratio high Mach number condition where the pressure difference between the inlet face and the adjacent fuselage surface was a maximum. A comparison of the results of this investigation with those of the sweptback inlet shows that differences in recovery $\bar{H}/H_o$ between the two configurations varied from 0 to 0.11 for mass-flow ratios m_i/m_o from 0.88 to 0.65, respectively, at a Mach number of 1.40; the recovery of the unswept inlet was higher than that of the swept configuration for $\frac{m_i}{m_o} < 0.88$. For the unswept inlet, the compressor-face pressure recovery varied from about 0.98 to 0.96 over the Mach number range from 0.65 to 1.40 at a mass-flow ratio of 0.65 for angles of attack of 0° and 4.2°. The changes in lift and pitching moment due to installation of the unswept inlet were generally small for the entire test range. Changes in drag were also small through the Mach number range at a mass-flow ratio of 0.80 at angles of attack of 0° and 4.2°. A comparison of the variation of drag with mass-flow ratio for the unswept- and sweptback-inlet configurations indicates that the "natural" bypassing of the boundary layer had no significant effect on drag.

INTRODUCTION

The results of investigations at transonic speeds of a series of sweptback wing-root inlets have been reported in references 1 to 4. These configurations, which were triangular, semielliptical, or semicircular, were installed in the root of a 45° sweptback wing. Inasmuch as several current and proposed airplanes are equipped with unswept wing-root inlets and the previous tests were limited to sweptback inlets, it was considered desirable to investigate the effects of inlet sweep on the internal and external aerodynamic characteristics. The purpose of the present tests, therefore, was to permit a direct comparison of the characteristics of an unswept inlet with those of a similar inlet which was swept back 45°.

The investigation, which was conducted in the Langley transonic blowdown tunnel, included measurements of the internal-flow characteristics and the changes in external forces due to the installation of a semielliptical inlet having zero sweep in the root of a 45° sweptback wing. These results are compared with those of the sweptback configuration and with those of the basic unducted model reported in reference 2.

SYMBOLS

H total pressure

$\frac{H - p_o}{H_o - p_o}$ impact pressure ratio

$\frac{p - p_o}{H_o - p_o}$ static-pressure coefficient

$\bar{H}/H_o$ integrated total-pressure recovery weighted with respect to mass flow, $\dfrac{\int_A \frac{\rho_1 V_1}{\rho_o V_o} \frac{H}{H_o} dA}{\int_A \frac{\rho_1 V_1}{\rho_o V_o} dA}$

m mass rate of internal flow

m_i/m_o mass-flow ratio, defined as the ratio of total internal mass flow to mass flow through free-stream tube with area equal to that of minimum projected frontal area of two inlets normal to flow direction

A	area
A_i	projected frontal area of both inlet openings normal to flow direction, defined by minimum inner-lip radius and fuselage wall
M	Mach number
C_{D_b}	drag coefficient of body alone, $\text{Drag}/q_o S$
$C_{D_{wb}}$	drag coefficient of basic wing-body combination, $\text{Drag}/q_o S$
$\Delta C_{D_{ext}}$	difference in drag coefficient obtained between basic and inlet configurations at same angle of attack and Mach number after effects of internal flow and air exit have been removed from inlet configuration (see appendix of ref. 1)
$C_{L_{wb}}$	lift coefficient of basic wing-body combination, $\text{Lift}/q_o S$
$\Delta C_{L_{ext}}$	difference in lift obtained between basic and inlet configurations at same angle of attack and Mach number after effects of internal flow and air exit have been removed from inlet configuration (see appendix of ref. 1)
$C_{m_{wb}}$	pitching-moment coefficient of basic configuration taken about quarter-chord position of mean aerodynamic chord, $\text{Moment}/q_o S\bar{c}$
ΔC_m	difference in pitching-moment coefficient obtained between basic and inlet configurations at same lift coefficient and Mach number after effects of air exit have been removed from inlet configuration
S	basic-wing area, 80.7 sq in.
q	dynamic pressure, $\frac{1}{2}\rho V^2$
V	velocity
c	local chord
$\bar{c}$	mean aerodynamic chord of basic wing, 4.462 in.
D	diameter
T_p	engine thrust based on corresponding total-pressure recovery

T_{ideal} engine thrust based on ideal total-pressure recovery, $\frac{\bar{H}}{H_o} = 1.00$

F frontal area of fuselage, 7.07 sq in.

R Reynolds number based on $\bar{c}$

X distance parallel to fuselage center line

Y distance perpendicular to a plane through wing chord

α angle of attack

ρ mass density

t wing thickness, percent total c

Subscripts:

c compressor-face station

i inlet

o free stream

x exit

MODELS

Basic Model

A plan-view photograph of the basic wing-body configuration investigated and reported in reference 2 is presented in figure 1(a). The model consisted of a wing with 45° quarter-chord sweep mounted with zero incidence in the midwing position on a fuselage of fineness ratio 6.7. The wing was composed of NACA 64A008 airfoil sections in the streamwise direction and had an aspect ratio of 4.032, a taper ratio of 0.6, no twist, and no dihedral (table I). The basic fuselage was formed by rotating an NACA 65_2A015 airfoil about its chord line.

Inlet Models

Provision for installation of the 45° sweptback semielliptical inlet of reference 2 (fig. 1(b)) was made by increasing the quarter-chord sweep, the thickness, and the chord of the basic wing in the inboard sections

(table I). The trailing-edge fillet resulting from the increase in chord increased the total wing area by 6.8 percent. A spanwise cross section of the frontal projection of the inlet taken at the line of maximum thickness was a semiellipse which was symmetrical about the chord line (table II). For the swept configuration of reference 2, the inlet was formed by cutting off the increased-chord-root sections along a line corresponding to the leading edge of the basic wing, and the inlet lips were faired around the semielliptical inlet shape from this new leading edge to the maximum-thickness line of the wing. The zero-sweep inlet of the present investigation (figs. 1(c) and 1(d)) was formed by adding plastic fairing strips to the swept-configuration model which extended forward from the line of maximum thickness. This extension increased the total wing area by about 3.4 percent. The inlet sections at the wing-body juncture and the frontal projection of the two inlets were identical (table II). The duct area for both configurations was constant up to the inlet measuring station. Inlet asymmetry and a lower lip stagger of 30° were incorporated to improve the external- and internal-flow performance, respectively, at high angles of attack.

The projected frontal area of the inlets relative to the fuselage $\left(\frac{A_i}{F} = 0.167\right)$ was the same as that for the triangular, semielliptical, and semicircular inlets tested in references 1, 2, and 3, respectively. Inasmuch as the inlets were assumed to admit the air flow for a single turbojet engine, the internal ducting was designed to undergo a cross-sectional transition from a semielliptical shape at the inlet to a semicircular shape and to merge at the assumed compressor face. The duct area was gradually increased to $1.115A_i$ between the inlet and compressor-face measuring station. The duct behind the compressor-face station was circular and led to an exit in the tail end of the fuselage. Four exit areas A_x/A_c of 1.0, 0.875, 0.750, and 0.625 were provided to vary the internal-flow rate (fig. 2).

APPARATUS AND METHODS

Pressure Measurements

The pressure instrumentation at the inlet and exit of the present model is indicated in figure 3. This arrangement was the same as that of reference 2 with the exception that the compressor-face pressure-tube instrumentation was omitted for the present investigation so that the model pressures and forces could be measured simultaneously. As described in reference 3, from a correlation of compressor-face and exit total pressures, it was determined that the loss factor between compressor face and exit was less than 2 percent of the free-stream stagnation pressure

through the range of test variables. Average total pressures equivalent to those at the compressor-face station were therefore obtained for the present inlet by adding the loss factor between stations to the average total-pressure ratios obtained at the exit.

Force Measurements

The model lift and drag forces and the pitching moment were measured with a three-component internal strain-gage balance. These data were corrected for the effects of internal flow, the jet exit, and sting interference in accordance with the methods presented in references 1 and 2.

Flow Study

The results of the investigation of the internal pressure-recovery characteristics and the external forces indicated that visual observations were needed to determine the nature of the flow ahead of the inlet measuring station. For these studies, schlieren photographs and an oil-flow technique were used. The oil-flow study consisted of placing oil droplets at various points on the surface of the model, in and around the inlet, and then photographing the motion of the droplets during the time that the tunnel was running and also after the run. The pattern made by the oil droplets indicated the flow direction within the boundary layer.

Tests and Accuracy

The tests were conducted in the Langley transonic blowdown tunnel at stagnation pressures ranging from 45 to 60 pounds per square inch absolute. The range of test variables and the estimated maximum error in the measured coefficients based on the scatter and repeatability of data points are given in the following tables:

Variable	Range	Maximum estimated error
M_o	0.65 to 1.40	±0.01
R	5.5×10^6 to 7.4×10^6	At any value of M_o, R varied ±2 percent because of variations in stagnation temperature
α	0° to 9.6°	$\pm 0.1^\circ$
m_i/m_o	0.54 to 0.91	±0.02

Measured coefficient	Maximum estimated error
$\Delta C_{L_{ext}}$	±0.01
$\Delta C_{D_{ext}}$	±0.001
ΔC_m	±0.003
$\frac{H - p_o}{H_o - p_o}$	±0.005
$\frac{\bar{H}}{H_o}$	±0.01

The large ratio of model-to-tunnel size precluded the attainment of force data which were exactly equivalent to free-air data at any test speed. At all supersonic speeds, the model forces were subject to the effects of tunnel-wall reflections of model compressions and expansions. These effects caused changes in drag coefficient with Mach number which were sometimes large and rather abrupt. As pointed out in reference 4, most of the effect of the wall-reflected disturbances on the drag of the wing-body configuration occurred on the body alone, so that subtraction of body-alone drag data from that of the wing-body combination resulted in variations of the drag characteristics with Mach number which were more nearly representative of the variations expected in free air. In any event, although the absolute force coefficients may not be correct, comparisons between the various configurations are believed to be correct to the given accuracy except for the range of Mach number from 1.08 to 1.22 where the reflections crossed the inboard regions of the wing. (See ref. 4.)

RESULTS AND DISCUSSION

Internal-Flow Characteristics

Contours of constant impact-pressure ratio at the inlet measuring station are presented in figure 4, and the average total-pressure recovery at the compressor-face station is presented in figure 5 for the range of test variables. Near-stream impact pressure was indicated over the inlet for all subsonic test conditions, with the exception of the regions affected by the entrance of the fuselage boundary layer. At supersonic speeds, the boundary-layer at the inlet measuring station thickened because of interaction of a shock wave located ahead of the

inlet and the boundary layer. As would be expected, the increase in boundary-layer thickness and the pressure losses across the shock effected reductions in average total pressure with increases in Mach number (see unswept inlet, fig. 5(b)). The variation of average total-pressure recovery with Mach number, however, was not as great at the low mass-flow ratio as at the high mass-flow ratio.

Inasmuch as the magnitude of shock boundary-layer interaction effects is greatly influenced by the condition of the boundary layer at the shock, that is, whether the boundary layer is turbulent or laminar, and inasmuch as the boundary layer ahead of the inlet on the full-scale airplane will most likely be turbulent, it is important to know the condition of the boundary layer ahead of the inlet in the present model tests. Repeat tests were made for a few representative test conditions, therefore, with boundary-layer transition artificially fixed near the fuselage nose, and the results showed that the addition of the transition strip had no measurable effect on the compressor-face total-pressure recovery. These results indicate, then, that the test Reynolds number (approximately 6.5×10^6 based on $\bar{c}$) was great enough to insure turbulent flow over the fuselage ahead of the inlet so that the model results should be representative of full-scale conditions.

The effect of increasing the angle of attack was to cause the losses due to the boundary layer to become asymmetrical, with the greater part concentrated in the lower regions of the inlet. (See fig. 4.) At Mach numbers of about 1.15 and below, variation of the angle of attack up to 9.6°, the maximum of the test, had no appreciable effect on the average pressure recovery (fig. 5(a)). At higher Mach numbers, the average recovery was essentially unaffected by changes in angle of attack up to 4.2°, about the normal cruise range of a fighter-type airplane.

The pressure recovery at both the inlet and compressor-face stations indicated that, at all test conditions, the recovery increased as the mass-flow ratio was reduced. This trend is contrary to that normally obtained with scoop-type inlets without boundary-layer-control devices (for example, see refs. 2 and 5). The usual trend without boundary-layer-control devices is for the pressure recovery to decrease with decreasing mass-flow ratio due to boundary-layer thickening as a result of a more severe adverse pressure gradient ahead of the inlet. (A counteracting trend of decreasing subsonic diffusion losses with a decrease in mass-flow ratio is usually small for well-designed diffusers.) Inasmuch as the usual pressure-recovery trend was not measured at either the inlet or compressor-face stations at either supersonic or subsonic speeds where the pressure losses at the inlet station are due to the boundary layer alone, it appeared that the measured variation of increasing pressure recovery with decreasing mass-flow ratio was strongly influenced by the boundary-layer flow. In order to study the flow phenomenon involved for the present unswept inlet, visual observations of the flow in the vicinity

of the inlet were made with the use of schlieren photographs and an oil-flow technique. (See section entitled "Apparatus and Methods".)

Schlieren photographs taken at Mach numbers from 1.19 to 1.40 are presented in figure 6 at mass-flow ratios from 0.59 to 0.84 for an angle of attack of 0°. At a Mach number of 1.19, it can be seen that a normal shock is located ahead of the inlet and that the boundary-layer thickness increases rapidly behind the wave. When the Mach number was increased to 1.30 or 1.40, a lambda-type shock was noted ahead of the inlet. Inasmuch as the fuselage boundary layer was turbulent, as previously noted, the lambda-type shock must be associated with turbulent separation. Close observation of the photographs also indicated that the expected increases in boundary-layer thickness and extent of separation occurred with decreases in mass-flow ratio, which again is opposite to the trend indicated by the pressure measurements at the inlet and engine-face station. At Mach numbers of 1.30 and above, a part of the trend of increasing pressure might be attributed to the more efficient compression ahead of the inlet at the lower mass-flow ratios; that is, increases in extent of a lambda-type shock, which accompanies increases in extent of separation, would be expected to result in higher total pressures behind the two-shock compression, as pointed out in reference 5 for the inlet with a boundary-layer scoop. The total-pressure contours at the inlet, however, do not show any significant changes in the outboard distribution nor in the maximum values as the mass-flow ratio is reduced (fig. 4). The contours, however, do show considerable improvement in the pressure ratios with a decrease in flow rate at the inboard sections of the inlet where the losses due to boundary layer would be greatest. It is noted that the contour $\frac{H_i - p_o}{H_o - p_o} = 0.95$ is quite near the inboard wall of the inlet for the lowest mass-flow ratio at $M_o = 1.40$. From this discussion, it would seem apparent that the trend of increasing total pressure with decreasing mass-flow ratio is primarily associated with a natural bypassing or aspiration of some part of the boundary layer. The amount of boundary-layer air bypassed probably increased with reductions in mass-flow ratio as a result of the increase in inlet static pressure with reductions in flow rate. This increase in inlet static pressure (fig. 4) would result in a greater pressure differential between the inlet flow and the external flow and would permit a greater amount of the separated boundary layer to flow to the lower pressure field on the fuselage.

An indication of the nature of the movement of the boundary layer in the vicinity of the inlet is shown by the oil-flow study in which the path indicated by the oil droplets defines the flow pattern in the lower part of the boundary layer; typical photographs at both subsonic and supersonic Mach numbers are presented in figure 7. It should be noted that the flow direction indicated in figure 7 was observed with the use of motion pictures made while the tunnel was running. The flow direction is best

seen in the enlarged photograph of figure 7(a). Here it is indicated that the boundary layer approached the inlet in a normal manner. At the front leg of the lambda-type shock (see fig. 6), the flow separated and began to be diverted around the inlet. Part of the flow in the region just ahead of the inlet moved forward from the inlet face to the field of lower pressure on the model fuselage, and the entering flow reattached; the line of reattachment, which lies slightly inside the inlet plane, can also be seen. The patterns were basically the same for all test conditions, subsonic as well as supersonic, as indicated in figures 7(b) and (c). That is, upon entering the adverse pressure field of the inlet, part of the boundary-layer flow diverted around the inlet and the entering flow reattached.

For the entire test range, the greater portion of the boundary layer tended to move around the lower inlet lip. (See fig. 7(a).) Due to this tendency, it appears that lip stagger may be an important factor in permitting the boundary layer to bypass the inlet. Furthermore, a survey of existing data on unswept scoop-type inlets without boundary-layer bypasses indicated that the trend of increasing recovery with decreasing mass-flow ratio was not noted but that these inlets incorporated little or no lip stagger. In one instance, the possibility of boundary-layer bypassing was noted for a scoop inlet without stagger (ref. 6), but in this case the total-pressure recovery remained about constant as the mass-flow ratio was decreased. It appears, then, that additional studies should be made of the effects of changes in lip stagger on the variations of scoop-inlet total-pressure recovery with inlet mass-flow ratio.

The average total-pressure recovery of the sweptback wing-root inlet presented in reference 2 and some previously unpublished data obtained during a more recent investigation of the same inlet configuration (ref. 4) are presented in figures 5(b) and (c) for comparison with the recovery of the unswept inlet. The variation of pressure recovery with mass-flow ratio for the swept inlet was opposite to that indicated for the unswept inlet, indicating that any boundary-layer bypassing around the swept inlet with decreasing mass-flow ratio must be of limited magnitude. As indicated in figure 5(b), this opposite trend affects the maximum differences in recovery $(0.11H_0)$ for the two configurations at the low mass-flow ratio (0.65) high Mach number (1.40) condition for angles of attack of 0° and 4.2°, the differences in recovery becoming almost negligible as the Mach number is decreased to subsonic values.

It will be noted in figure 5(c) that, at supersonic Mach numbers, the recovery of the swept inlet is higher than that of the unswept inlet for the high test mass-flow ratios. This difference in recovery is attributed largely to the fact that values of local pressure as much as $0.03H_0$ greater than normal-shock recovery were measured (according to unpublished data of ref. 2) in the outboard sections of the swept inlet in contrast with normal-shock values for the unswept inlet. It is

concluded, therefore, that the wave ahead of the outboard sections of the swept inlets was inclined rather than normal, with associated reductions in losses through the wave. At the higher mass-flow ratios, then, the reduced losses through the inclined wave ahead of the sweptback inlet are probably more significant than the improvement in recovery associated with boundary-layer bypassing for the unswept configuration.

External-Flow Characteristics

Lift and pitching moment.- The lift and pitching-moment characteristics of the unswept inlet are presented in figures 8 and 9, respectively, at a mass-flow ratio of 0.8. Data for the sweptback-inlet configuration and the basic wing-body configuration (ref. 2) are presented for comparison. The effects of differences in model configuration on lift coefficient (fig. 8) were almost insignificant through the test Mach number range at angles of attack up to approximately 7°. At higher angles of attack, the unswept inlet had slightly lower lift at Mach numbers from about 0.90 to 1.05; these angles, however, are greater than that required for pitch-up. (See fig. 9.)

The addition of either the unswept or sweptback inlet to the basic configuration had no significant adverse effects on the static longitudinal stability (fig. 9) for the entire test range; in fact, an increase in stability is noted at Mach numbers near unity. Pitch-up for the unswept inlet occurred at about the same lift coefficient but was somewhat more abrupt than for the basic and sweptback inlet configurations. The effect of variations in mass-flow ratio on the lift and pitching-moment coefficients was negligible for both inlet configurations (this effect is not shown in figs. 8 and 9).

Drag.- As pointed out earlier, the drag coefficients of the basic body alone have been subtracted from those of both the inlet and basic wing-body configuration to obtain variations with Mach number which are more nearly representative of drag-coefficient variations in free air. The external-drag coefficients for the basic wing-body configuration and those for the basic wing-body configuration, plus the drag increments due to the installation of the sweptback and the unswept inlets are presented in figure 10 as a function of Mach number and inlet mass-flow ratio at angles of attack of 0°, 4.2°, and 9.6°. Installation of either inlet generally had about the same effect on external drag through the entire test range of Mach number at a mass-flow ratio of 0.80 for angles of attack of 0° and 4.2°. At 0° and 4.2°, the maximum increase in drag for both inlet configurations (as compared with that of the basic wing-body configuration) was effected at Mach numbers slightly higher than 1.0. The largest drag differences due to inlet installation were effected at an angle of attack of 9.6°, the maximum of the test. These differences are considered to be unimportant since they occur beyond the normal operational angles of attack.

As was previously discussed in the section entitled "Apparatus and Methods", the drag increments are not valid in the Mach number range between about 1.08 and 1.22 because of tunnel-wall interference effects. The drag data, therefore, are not presented for this Mach number range.

As may be seen in figure 10(b), the drag of the two inlet configurations is, in general, about the same for a given value of mass-flow ratio and Mach number for the entire range of mass-flow ratio; the rate of change of drag with mass-flow ratio also is about the same for the two configurations. Important increases in slope might have been expected with decreases in mass-flow ratio for the unswept configuration, inasmuch as the bypassing of the boundary layer was more complete at low mass-flow ratios (see fig. 5(c)). It appears, however, that the bypassing of the boundary layer ahead of the unswept inlet had no significant effect on external drag.

Inlet-Performance Comparisons

An overall evaluation of any air-induction system depends on both the total-pressure characteristics and on the external-drag increment incurred by installation of the system. For the purpose of comparing the performance of the unswept inlet of the present investigation and the sweptback inlet of reference 2, however, it was considered necessary to evaluate only the effects of the total-pressure characteristics because, as indicated previously, the drag increments incurred with installation of the two inlets were essentially the same at given values of inlet mass-flow ratio and Mach number at the lower angles of attack. In order that the comparisons between the two inlets might be based on a parameter more closely related to flight programs than on a direct comparison of the total-pressure recovery (fig. 5(b)), the losses in total pressure were converted to equivalent losses in engine thrust for two schedules of variation of inlet mass-flow ratio with Mach number. Two mass-flow-ratio schedules (fig. 11(a)) were selected so that the effects of the unusual total-pressure-ratio differences between the two inlets could be clearly indicated; the design values were $m_i/m_o = 0.65$ and 0.80 at $M_o = 1.40$. The engine thrust characteristics are presented in figure 11(b) and 11(c) in the form of the ratio of net engine thrust to the ideal (100-percent pressure recovery) engine thrust T_p/T_{ideal}. The net engine thrust ratios for the two inlets were obtained by conversion of the measured total-pressure losses to equivalent losses in engine thrust through the use of a curve similar to that presented in reference 7. It should be noted that the net thrust ratios for the high mass-flow ratios of figure 11 were obtained by extrapolating the curves of total-pressure recovery plotted against mass-flow ratio (fig. 5(c)) a small amount; it was assumed that total-pressure losses due to inlet choking were initiated at a mass-flow ratio of 0.95, and the data were not extrapolated beyond this value.

At the lower mass-flow-ratio design (fig. 11(c)), both inlets had net thrust ratios of 0.95 or greater for Mach numbers of 1.0 and below. With increases in Mach number, however, the ratio for the sweptback inlet decreased steadily, reaching a value of about 0.82 at $M_0 = 1.40$, whereas the ratio for the unswept inlet remained slightly above 0.95 for the entire range. At the higher mass-flow-ratio design (fig. 11(b)), the differences in net thrust ratio between the two inlets at the higher Mach numbers were decreased. At the design Mach number of 1.40, the net thrust ratios were 0.91 and 0.87 for the unswept and sweptback inlets, respectively. For both inlets, the higher design flow ratio would produce inlet choking at a substantially higher Mach number (fig. 11(a)) and, therefore, the losses in thrust ratio at low speeds would probably be greater because of the internal shock losses and a reduction in allowable engine air flow.

Although comparisons have been made between the two inlets for each of the selected mass-flow-ratio schedules, it would be of interest, now, to compare the effect of design mass-flow ratio on the performance of each inlet. To do this, consideration must be given to the difference in external drag associated with the different mass-flow ratios and with the different inlet area required for a given engine. It can be seen from figure 11 that, for the unswept inlet, if the thrust decrement equivalent to the drag increase caused by changing the design mass-flow ratio from 0.80 to 0.65 is less than about 5 percent of the ideal engine thrust at $M_0 = 1.40$, the lower design mass-flow ratio will have a small advantage in net thrust output as compared with the higher design mass-flow ratio. As previously indicated, the lower design mass-flow ratio would have the added advantage of delay of inlet choke to a lower Mach number (fig. 11(a)) and associated better low-speed performance. Even if the drag differences were such as to eliminate the advantage in net thrust output at the low mass-flow-ratio design as compared with the high mass-flow ratio design, the latter advantage of a low mass-flow-ratio design would still be an important consideration. It is obvious that, for the sweptback inlet, the performance at the low design mass-flow ratio is inferior to that at the high design mass-flow ratio, inasmuch as a decrease in mass-flow ratio adversely affects the pressure recovery (fig. 5(c)) as well as the drag (fig. 10(b)); the effect on drag of the required change in inlet area is also adverse with a decrease in design mass flow ratio. Inasmuch as figure 11(b) indicates that, at Mach numbers greater than 1.2, the performance of the unswept inlet is higher than that of the sweptback inlet at the high design mass-flow ratio $\left(\Delta C_{D_{ext}} \text{ the same for both inlets}\right)$ and because the performance of the unswept inlet increases with decreasing design mass-flow ratio, as indicated previously, it seems logical that the performance of the unswept inlet at the low design mass-flow ratio is superior to that of the sweptback inlet for the range of design mass-flow ratio between 0.65 and 0.80 for a design Mach number of 1.40. It should be mentioned, however, that

the comparison between the two inlets may be entirely different at higher Mach numbers ($M_o > 1.40$). The comparison may also be different in the present range of Mach number if improvements in total-pressure recovery characteristics for the sweptback-inlet configuration can be obtained through use of an efficient boundary-layer-control system.

SUMMARY OF RESULTS

An investigation has been made in the Langley transonic blowdown tunnel to study the internal and external aerodynamic characteristics of an unswept semielliptical air intake installed in the root of a 45° sweptback wing. The results of this investigation have been compared with those of a similar inlet which was swept back along the wing leading edge. Tests were made through a Mach number range from 0.65 to 1.40 at mass-flow ratios of 0.55 to 0.90 and angles of attack from 0° to 9.6°. The more important results are summarized as follows:

1. Increases in compressor-face total-pressure recovery $\bar{H}/H_o$ with decreases in inlet mass-flow ratio m_i/m_o were effected at all test conditions. This trend was attributed to a "natural" bypassing of a large part of the boundary-layer flow around the lower lip which was staggered 30°. The bypassing was more complete at the low mass-flow ratio high Mach number condition.

2. The variation of total-pressure recovery with mass-flow ratio for the unswept inlet was opposite to that for the sweptback inlet through the test range of mass-flow ratio. The difference in recovery $\bar{H}/H_o$ between the two inlets at a Mach number of 1.40 varied from 0 to 0.11 for a change in m_i/m_o from 0.88 to 0.65, respectively; the recovery of the unswept inlet was higher than that of the swept configuration at $\frac{m_i}{m_o} < 0.88$.

3. The compressor-face total-pressure recovery for the unswept inlet varied from about 0.98 to 0.96 through the Mach number range from 0.65 to 1.40 at a mass-flow ratio of 0.65 for angles of attack of 0° and 4.2°; normal shock recovery was indicated at $M_o = 1.40$.

4. The effect of installation of the unswept inlet on the lift, drag, and pitching moment was about the same as the effect of installation of the sweptback inlet for the entire test range of mass-flow ratio and Mach number at normal operational angles of attack.

5. A comparison of the variation of drag with mass-flow ratio for the unswept- and sweptback-inlet configurations indicates that the "natural" bypassing of the boundary layer had no significant effect on drag.

Langley Aeronautical Laboratory,
National Advisory Committee for Aeronautics,
Langley Field, Va., June 13, 1955.

REFERENCES

1. Howell, Robert R., and Keith, Arvid L., Jr.: An Investigation at Transonic Speeds of the Aerodynamic Characteristics of an Air Inlet Installed in the Root of a 45° Sweptback Wing. NACA RM L52H08a, 1952.

2. Howell, Robert R., and Trescot, Charles D., Jr.: Investigation at Transonic Speeds of Aerodynamic Characteristics of a Semielliptical Air Inlet in the Root of a 45° Sweptback Wing. NACA RM L53J22a, 1953.

3. Trescot, Charles D., Jr., and Keith, Arvid L., Jr.: Investigation at Transonic Speeds of Aerodynamic Characteristics of a Semicircular Air Inlet in the Root of a 45° Sweptback Wing. NACA RM L55A05a, 1955.

4. Keith, Arvid L., Jr.: Transonic Wind-Tunnel Investigation of the Effects of Body Indentation on the Aerodynamic Characteristics of a Semielliptical Sweptback Wing-Root Inlet Configuration. NACA RM L54A29, 1954.

5. Frazer, Alson C., and Anderson, Warren E.: Performance of a Normal-Shock Scoop Inlet With Boundary-Layer Control. NACA RM A53D29, 1953.

6. Boswinkle, Robert W., Jr., and Mitchell, Meade H., Jr.: Experimental Investigation of Internal-Flow Characteristics of Forward Underslung Fuselage Scoops With Unswept and Sweptback Entrances at Mach Numbers of 1.41 to 1.96. NACA RM L52A24, 1952.

7. Schueller, Carl F., and Esenwein, Fred T.: Analytical and Experimental Investigation of Inlet-Engine Matching for Turbojet-Powered Aircraft at Mach Numbers Up to 2.0. NACA RM E51K20, 1952.

TABLE I.- DESIGN DIMENSIONS OF BASIC AND DUCTED WING

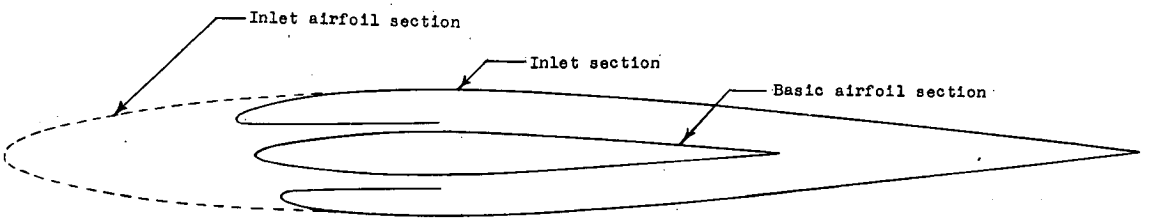

Semispan wing station (in.) from fuselage ℄	Basic wing			Ducted wing						
				Inlet airfoil section			45° Swept inlet		Zero swept inlet	
	c (in.)	t (percent c)	c/4 sweep	Total c (in.) (a)	t (percent total c)	c/4 sweep	Inlet c (in.)	t (percent inlet c)	Inlet c (in.)	t (percent inlet c)
0	5.587	8	45°							
1.347	5.250	8	45°	11.250	11.11	60°	8.777	14.24	8.777	14.24
1.500	5.212	8	45°	10.522	11.80	60°	8.334	14.90	8.497	14.61
1.750	5.150	8	45°	9.331	12.83	60°	7.608	15.75	8.037	14.89
2.000	5.087	8	45°	8.141	13.59	60°	6.883	16.07	7.578	14.60
2.250	5.025	8	45°	6.951	13.74	60°	6.157	15.53	7.118	13.42
[b]2.455	4.973	8	45°	5.976	12.78	60°	5.562	13.74	6.737	11.34
2.677	4.918	8	45°	4.918	8.00	60°	4.918	8.00	4.918	8.00
3.000	4.837	8	45°	4.837	8.00	45°	4.873	8.00	4.837	8.00
3.284	4.766	8	45°	4.766	8.00	45°	4.766	8.00	4.766	8.00
3.347	4.750	8	45°	4.750	8.00	45°	4.750	8.00	4.750	8.00
4.500	4.462	8	45°	4.462	8.00	45°	4.462	8.00	4.462	8.00
9.000	3.337	8	45°	3.337	8.00	45°	3.337	8.00	3.337	8.00

(a) Chord before installation of inlet.
(b) Outboard end of inlet.

TABLE II.- DESIGN COORDINATES FOR INTERNAL AND EXTERNAL LIPS OF 0° AND 45° SWEPT INLETS

[All dimensions are in inches]

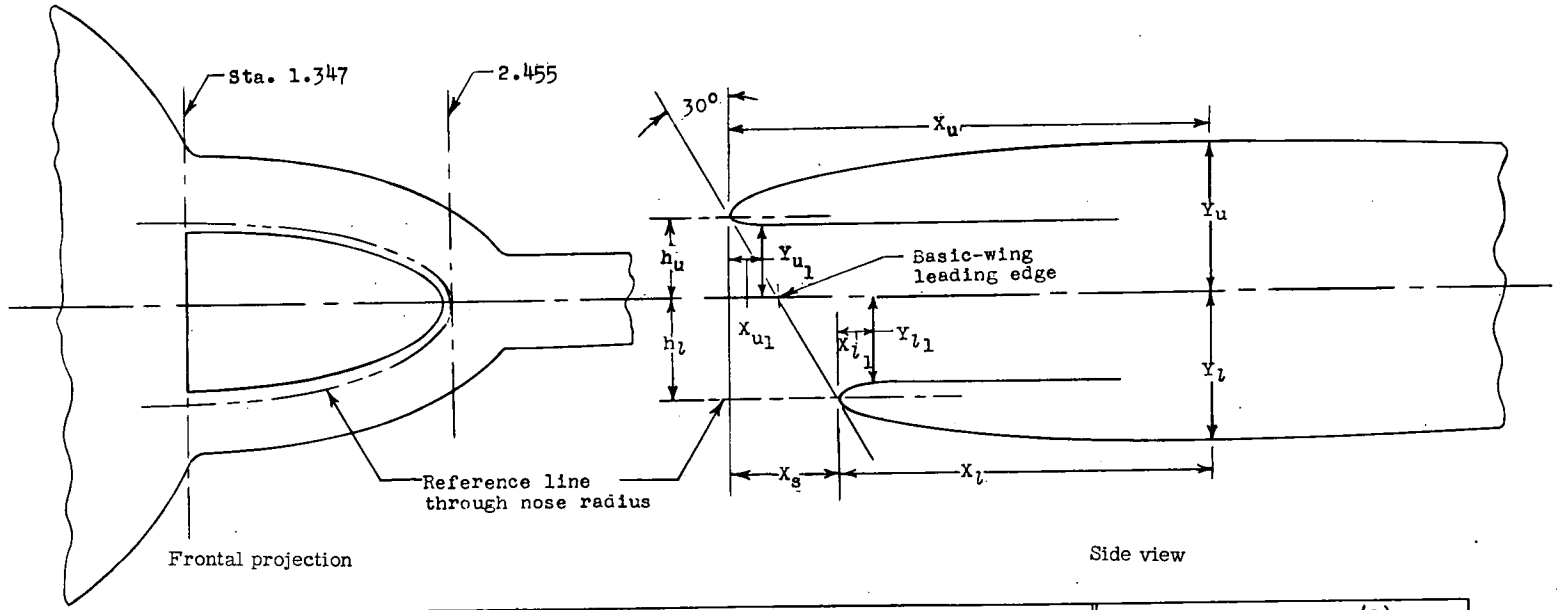

Wing station	External surfaces (a)									Internal surfaces (a)			
	h_u	h_l	X_s	Y_u	Y_l	45° swept		Zero swept		X_{u_1}	Y_{u_1}	X_{l_1}	Y_{l_1}
						X_u	X_l	X_u	X_l				
1.347	0.338	0.428	0.442	0.625	0.626	1.998	1.556	1.998	1.556	0.125	0.300	0.185	0.366
1.500	.334	.423	.437	.621	.621	2.003	1.567	2.166	1.730	.125	.296	.185	.361
1.750	.314	.398	.411	.599	.599	2.004	1.593	2.433	2.022	.125	.278	.185	.338
2.000	.273	.345	.357	.553	.553	1.991	1.635	2.686	2.330	.125	.238	.185	.289
2.250	.195	.248	.256	.478	.478	1.960	1.705	2.921	2.666	.125	.161	.185	.196

(a) External and internal nose shapes determined from elliptical ordinates.

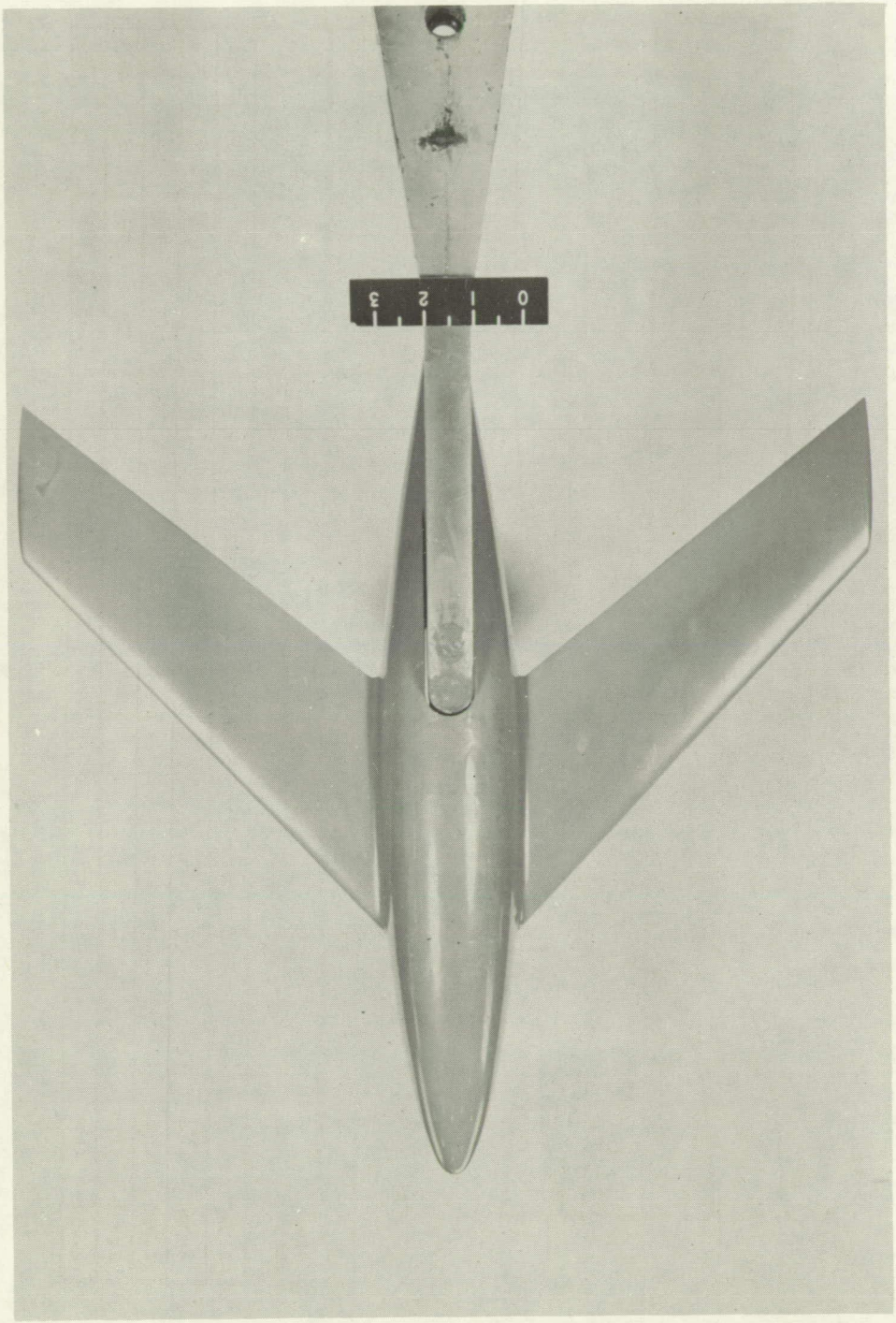

L-78978

(a) Plan view of basic model (ref. 2).

Figure 1.- Photographs of basic model and 0° and 45° sweptback-inlet configurations.

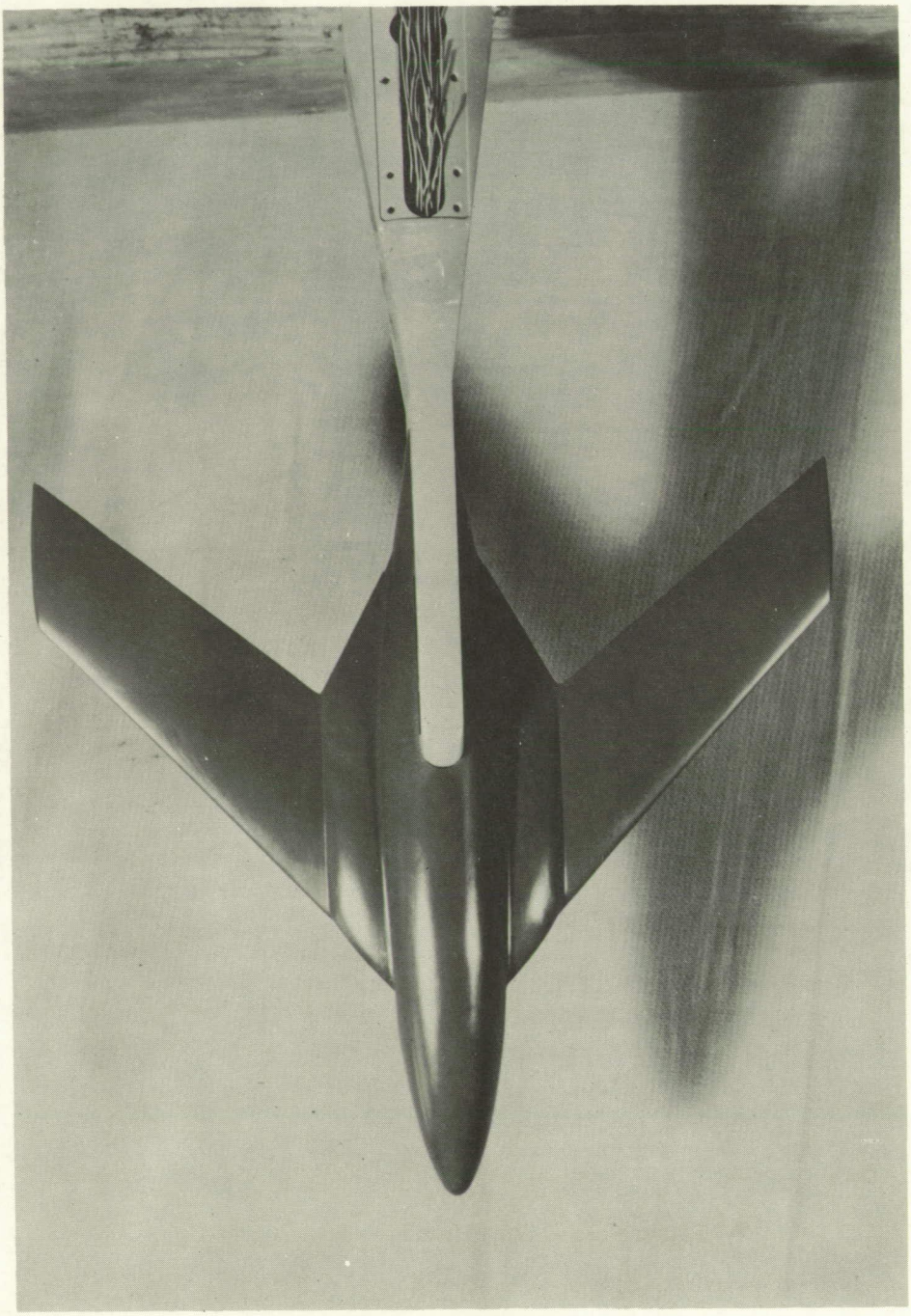

L-76796

(b) Plan view of upper surface of swept-inlet configuration (ref. 2).

Figure 1.- Continued.

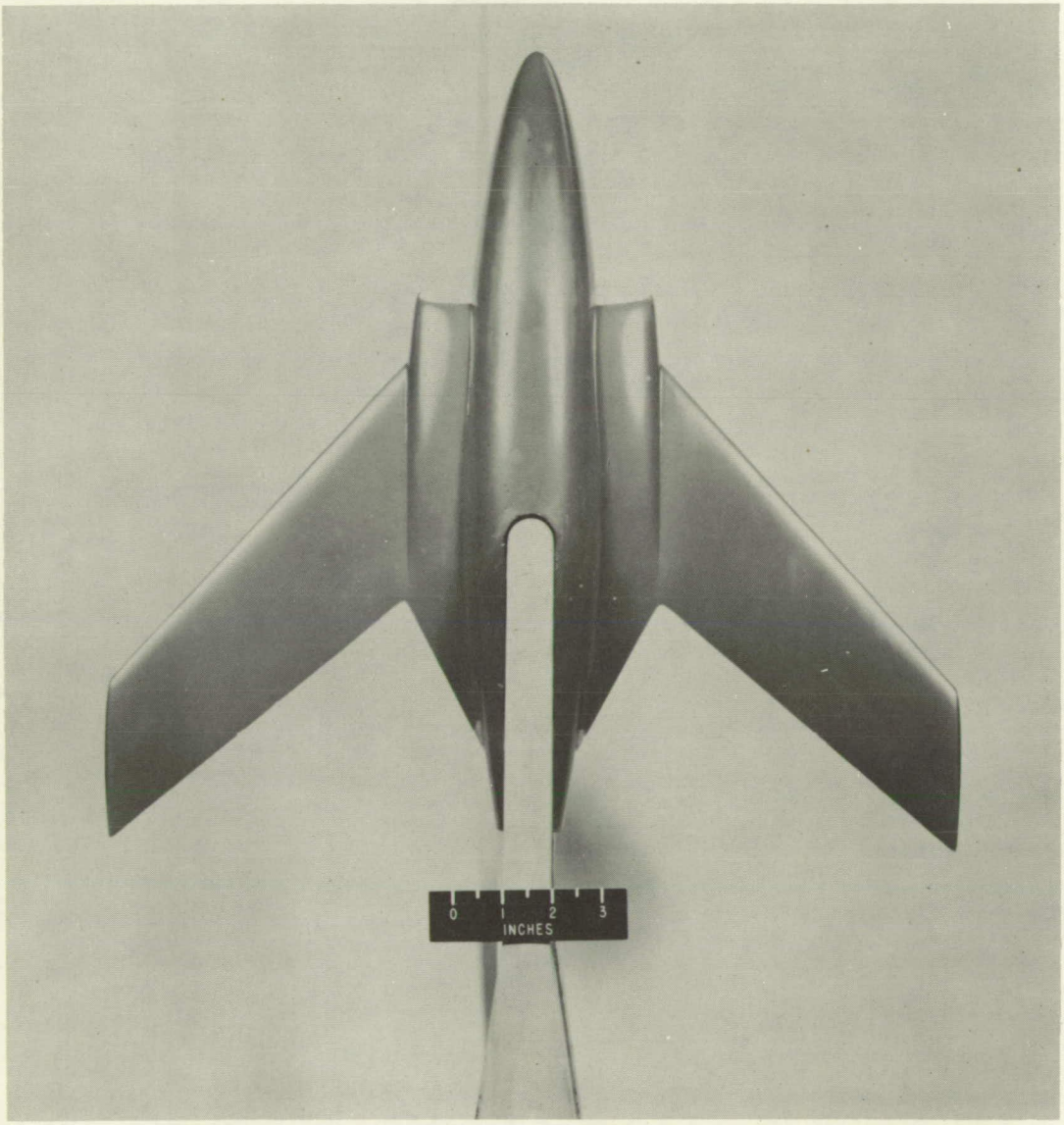

L-82980

(c) Plan view of lower surface of unswept-inlet configuration.

Figure 1.- Continued.

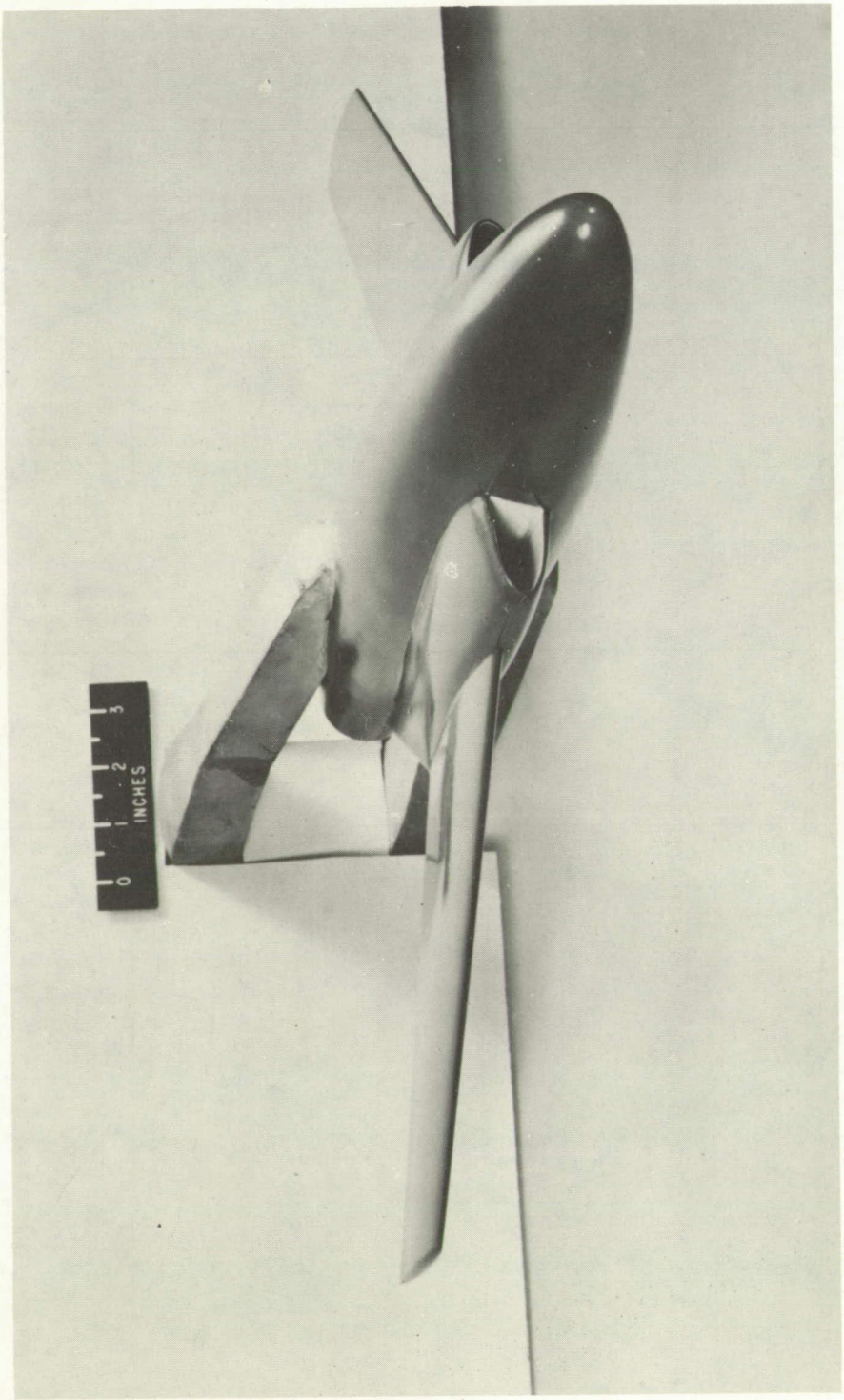

L-82981

(d) Three-quarter front view of unswept-inlet configuration.

Figure 1.- Concluded.

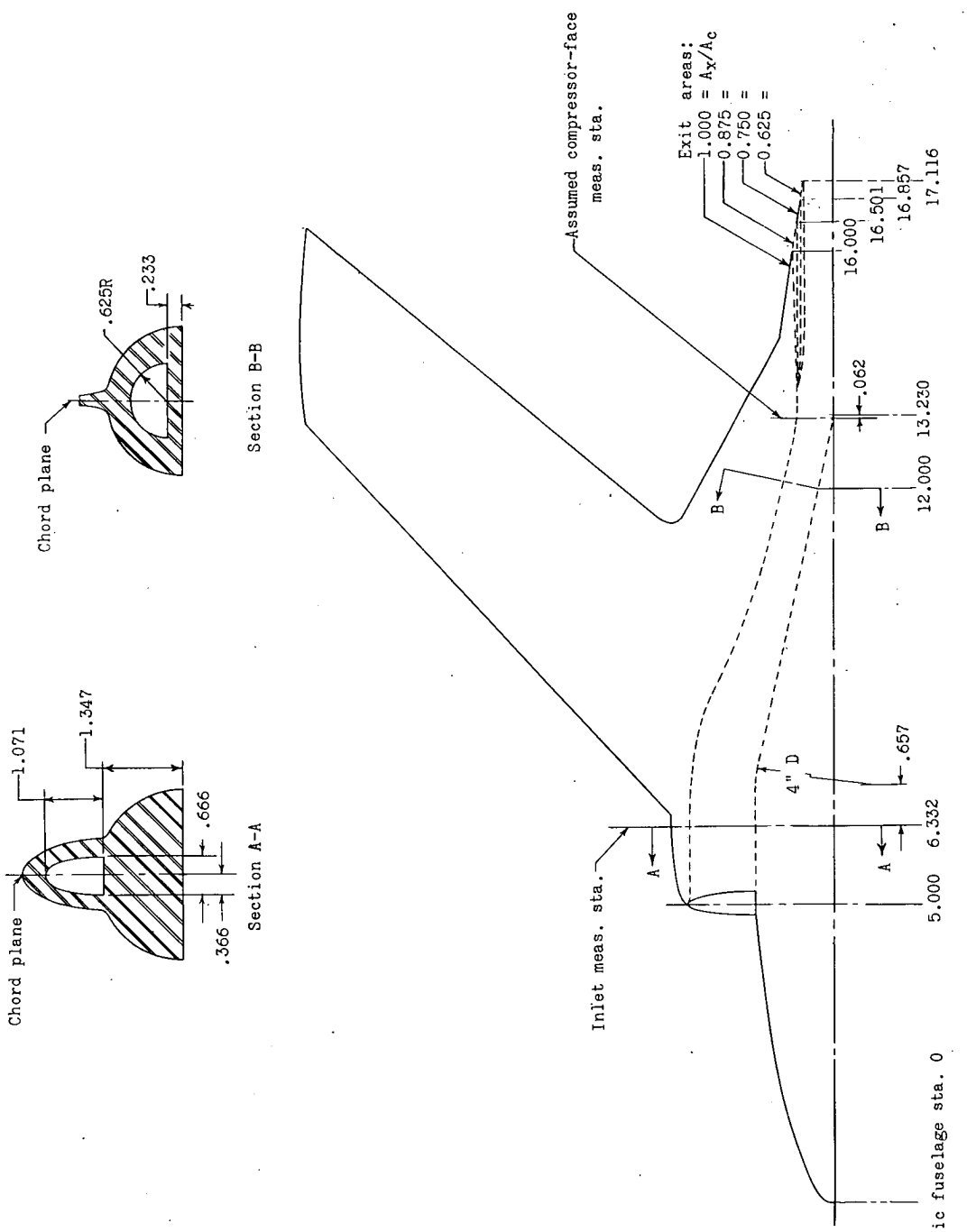

Figure 2.- Plan view of 0° swept-inlet configuration showing internal duct and exits. All dimensions are in inches.

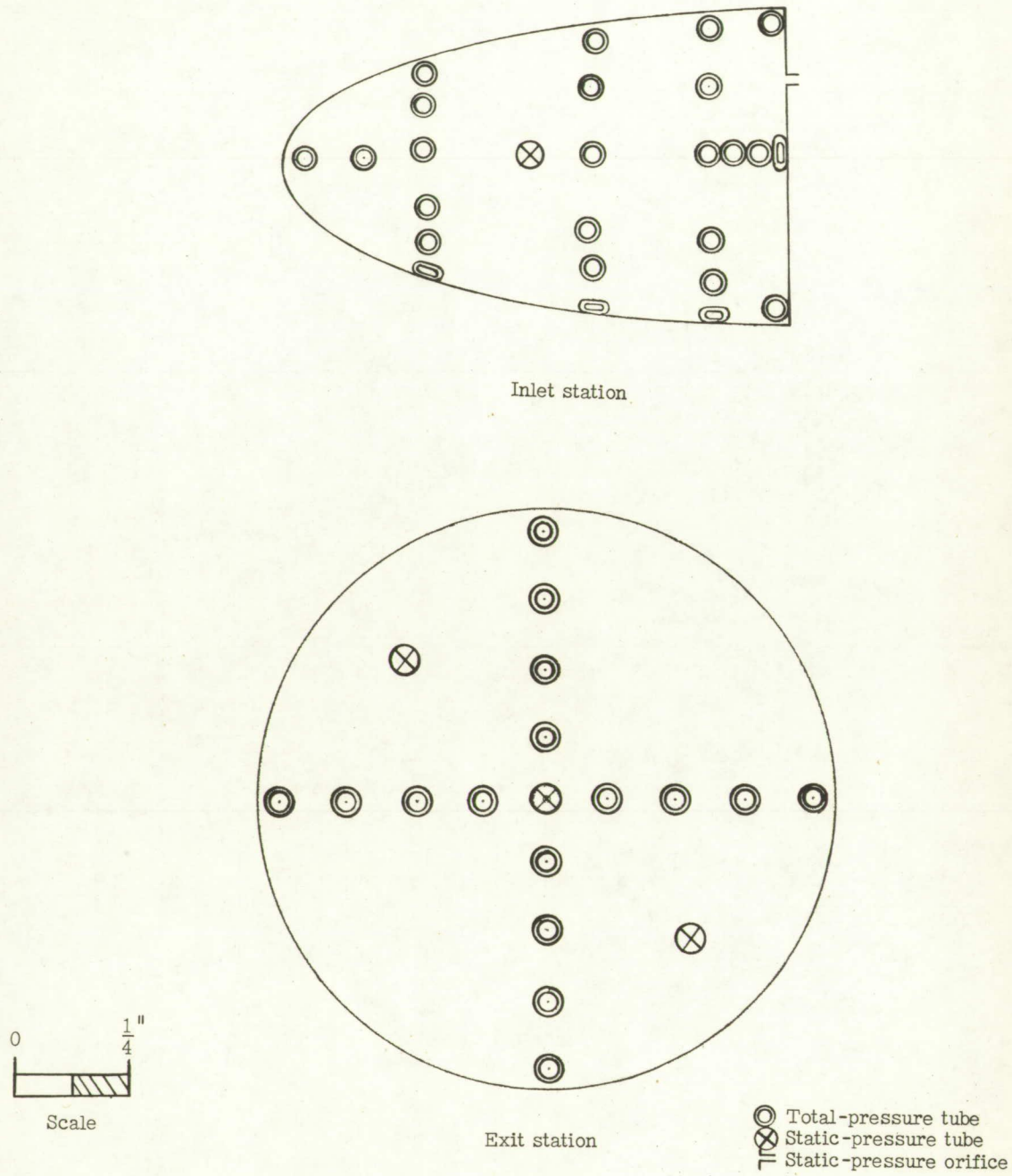

Figure 3.- Distribution of total- and static-pressure tubes at inlet and exit stations.

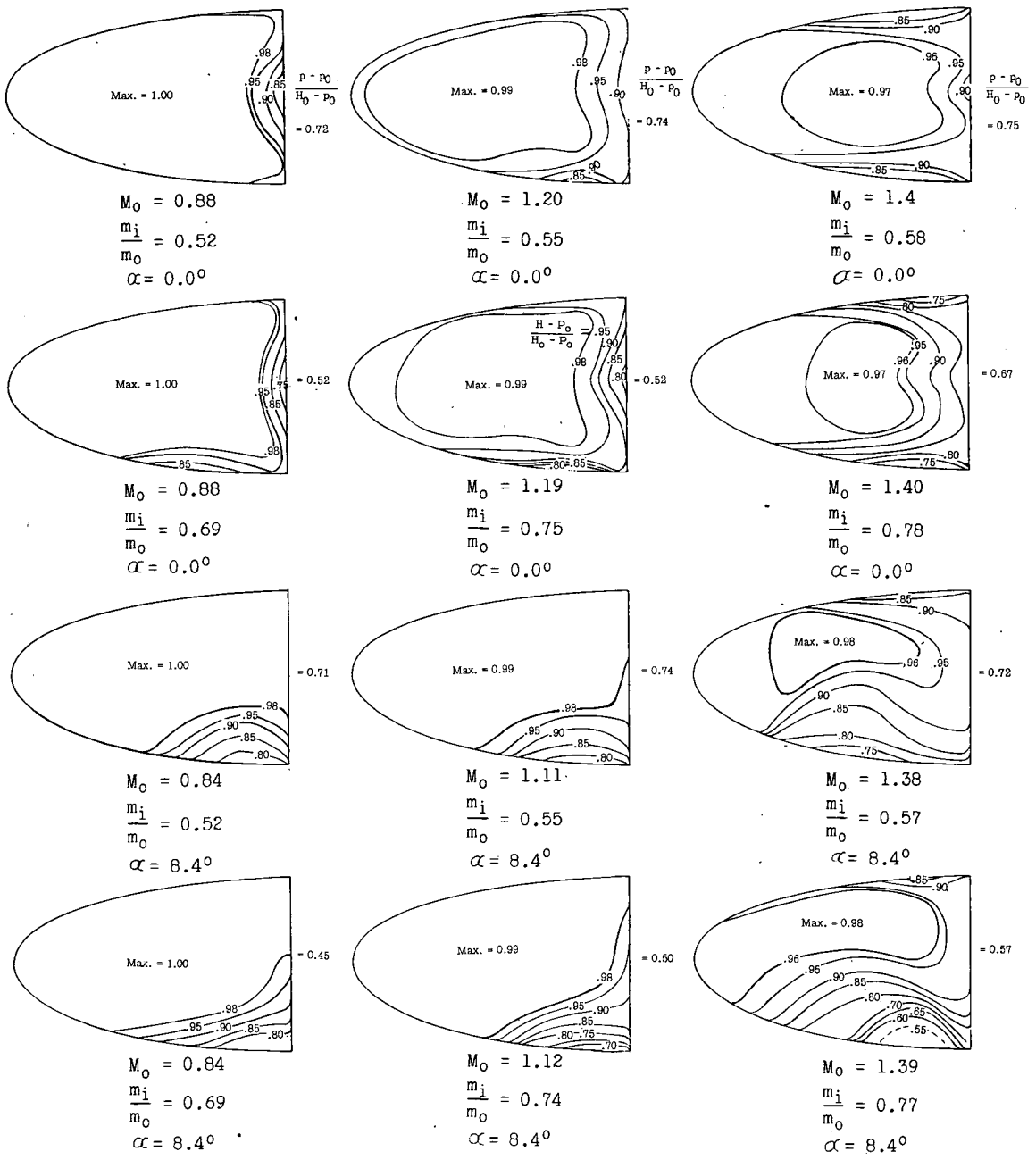

Figure 4.- Contours of constant impact-pressure ratio at inlet measuring station.

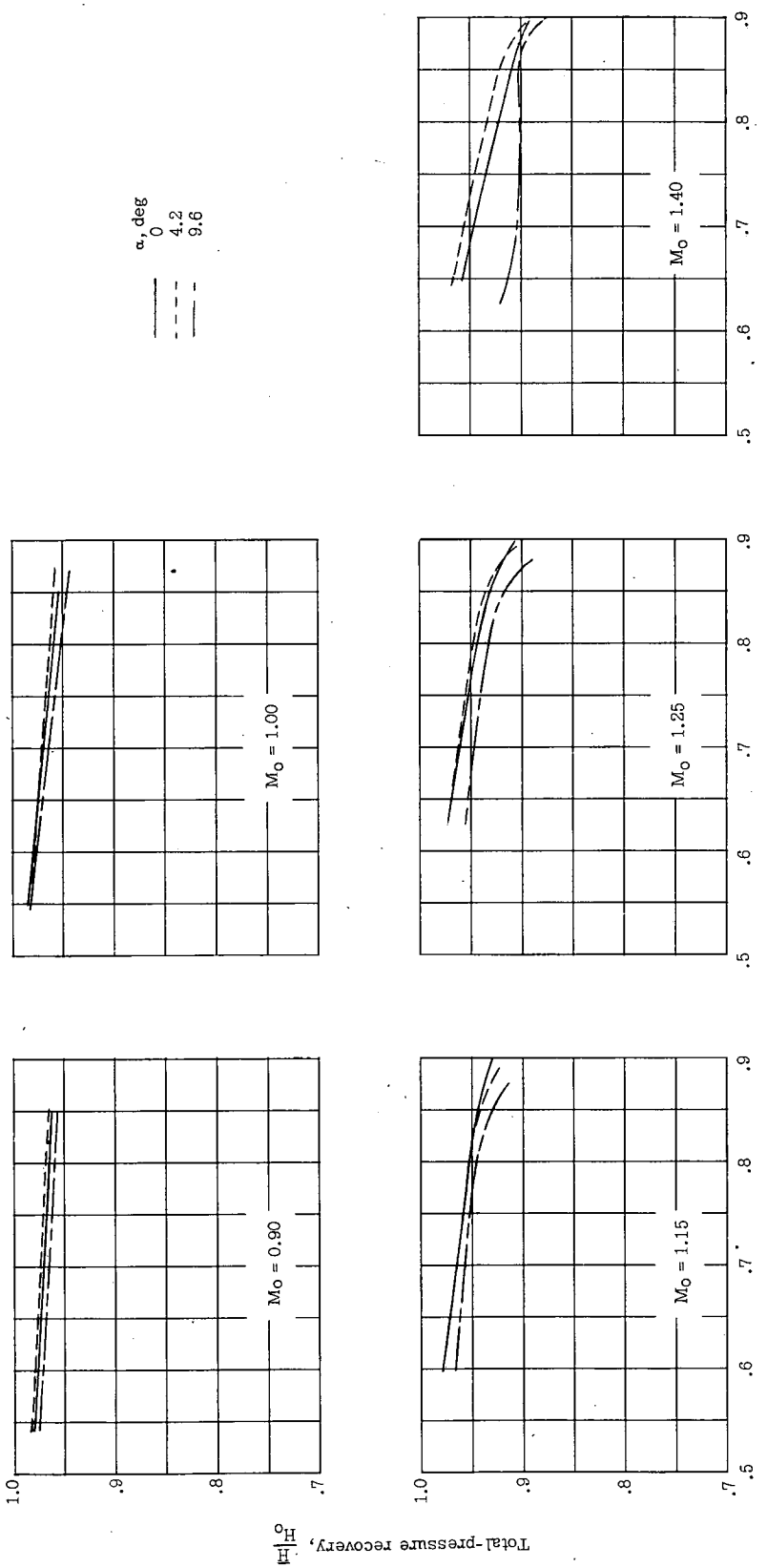

(a) Effect of variations in mass-flow ratio.

Figure 5.- Effect of variations in mass-flow ratio, Mach number, and angle of attack on total-pressure recovery at compressor face.

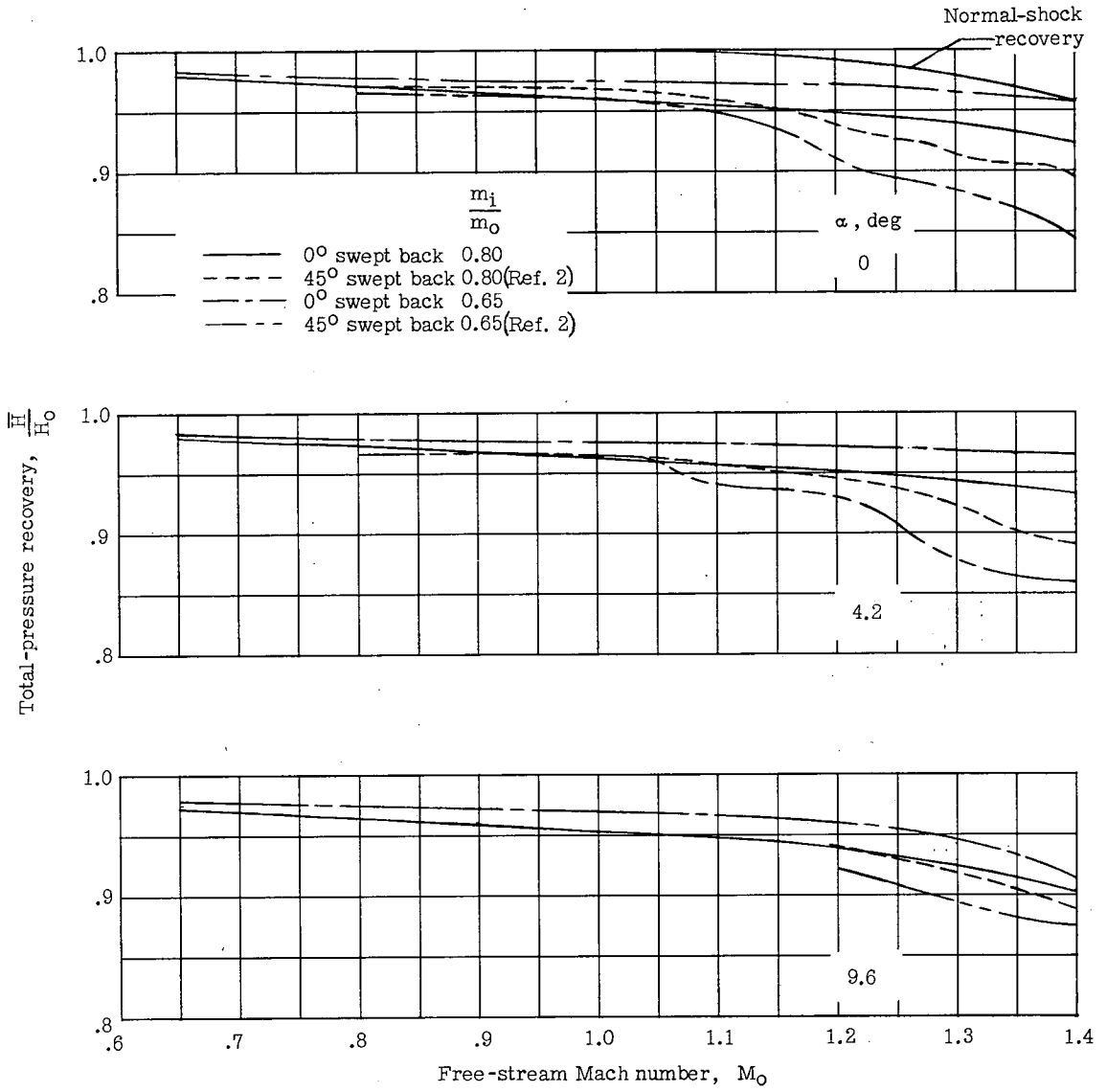

(b) Effect of variations in Mach number and angle of attack.

Figure 5.- Continued.

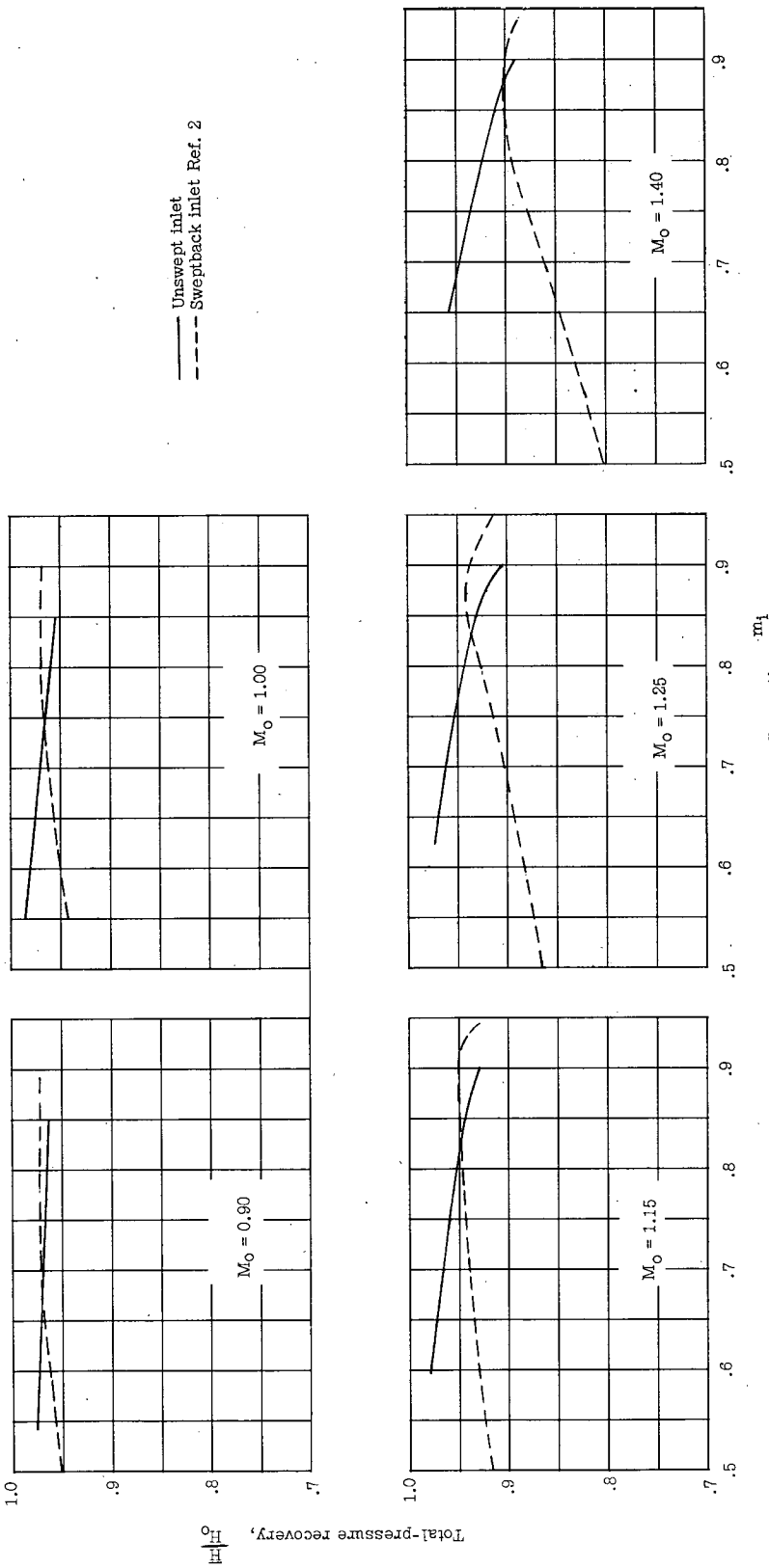

(c) Comparison of effect of variations in mass-flow ratio on total-pressure recovery at compressor face for unswept and sweptback inlets. $\alpha = 0^\circ$.

Figure 5.- Concluded.

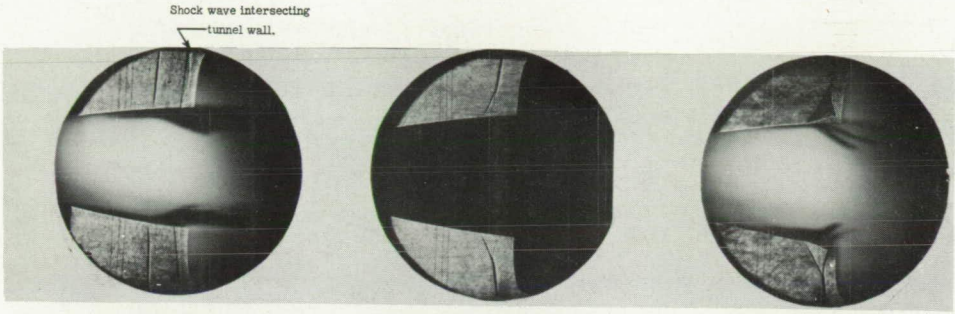

$M_o = 1.19$ $\frac{m_i}{m_o} = 0.59$ $\alpha = 0.0°$

$M_o = 1.30$ $\frac{m_i}{m_o} = 0.61$ $\alpha = 0.0°$

$M_o = 1.40$ $\frac{m_i}{m_o} = 0.63$ $\alpha = 0.0°$

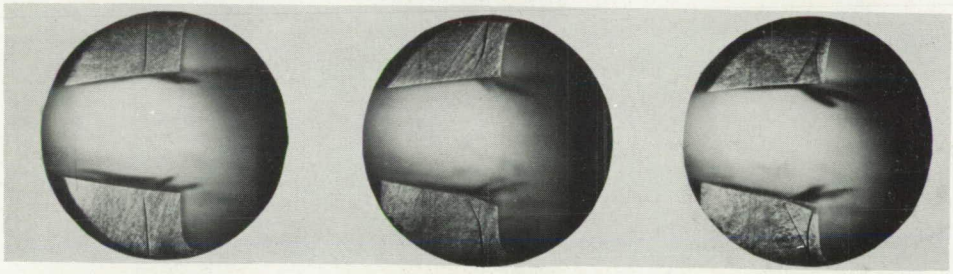

$M_o = 1.19$ $\frac{m_i}{m_o} = 0.69$ $\alpha = 0.0°$

$M_o = 1.30$ $\frac{m_i}{m_o} = 0.72$ $\alpha = 0.0°$

$M_o = 1.40$ $\frac{m_i}{m_o} = 0.74$ $\alpha = 0.0°$

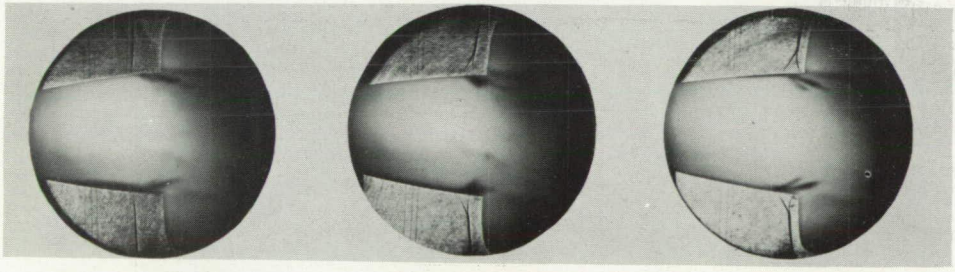

$M_o = 1.19$ $\frac{m_i}{m_o} = 0.81$ $\alpha = 0.0°$

$M_o = 1.30$ $\frac{m_i}{m_o} = 0.82$ $\alpha = 0.0°$

$M_o = 1.40$ $\frac{m_i}{m_o} = 0.84$ $\alpha = 0.0°$

L-89341

Figure 6.- Schlieren photographs taken at Mach numbers from 1.19 to 1.40 and mass-flow ratios from 0.59 to 0.84.

L-84634.1

(a) Close-up view. M = 1.40, m_i/m_o = 0.74.

Figure 7.- Oil-flow-study photographs indicating direction of boundary-layer flow. $\alpha = 0.0^{\circ}$.

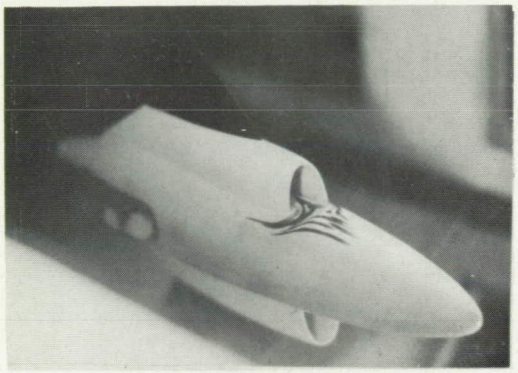

$M_o = 0.87$

$m_i/m_o = 0.55$

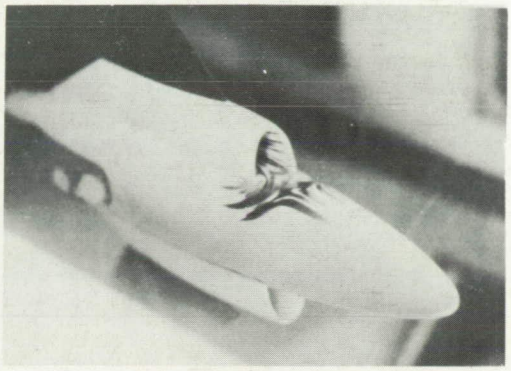

$M_o = 1.19$

$m_i/m_o = 0.59$

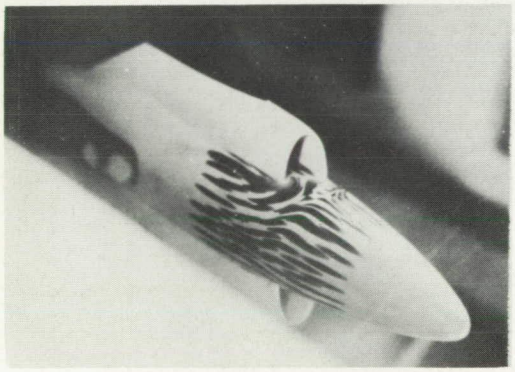

$M_o = 1.19$

$m_i/m_o = 0.69$

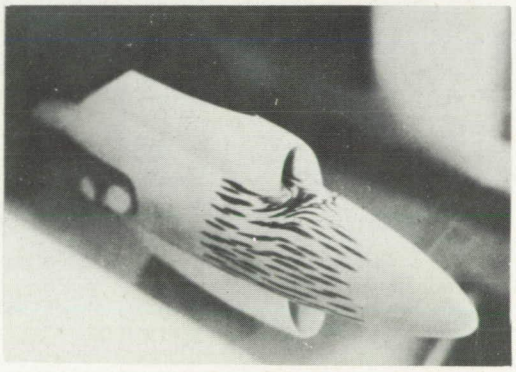

$M_o = 1.19$

$m_i/m_o = 0.81$

L-89342

(b) $M_o = 0.87$ and 1.19.

Figure 7.- Continued.

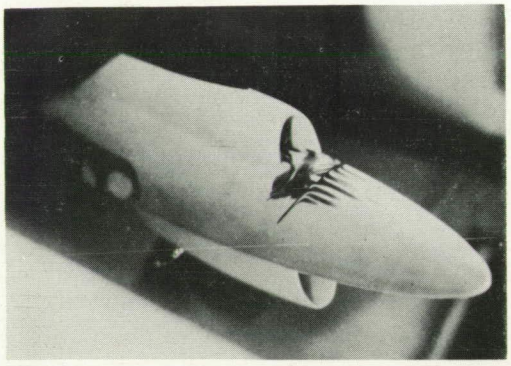

$M_o = 1.40$

$m_i/m_o = 0.63$

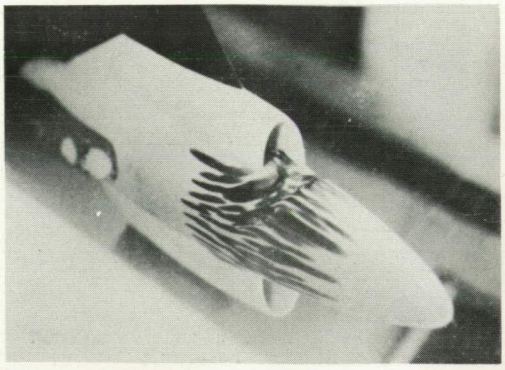

$M_o = 1.40$

$m_i/m_o = 0.74$

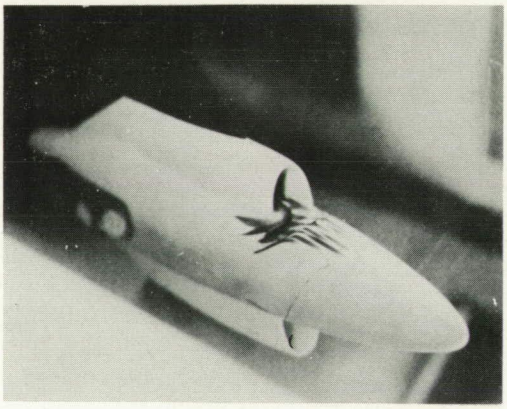

$M_o = 1.40$

$m_i/m_o = 0.84$

L-89343

(c) $M_o = 1.40$.

Figure 7.- Concluded.

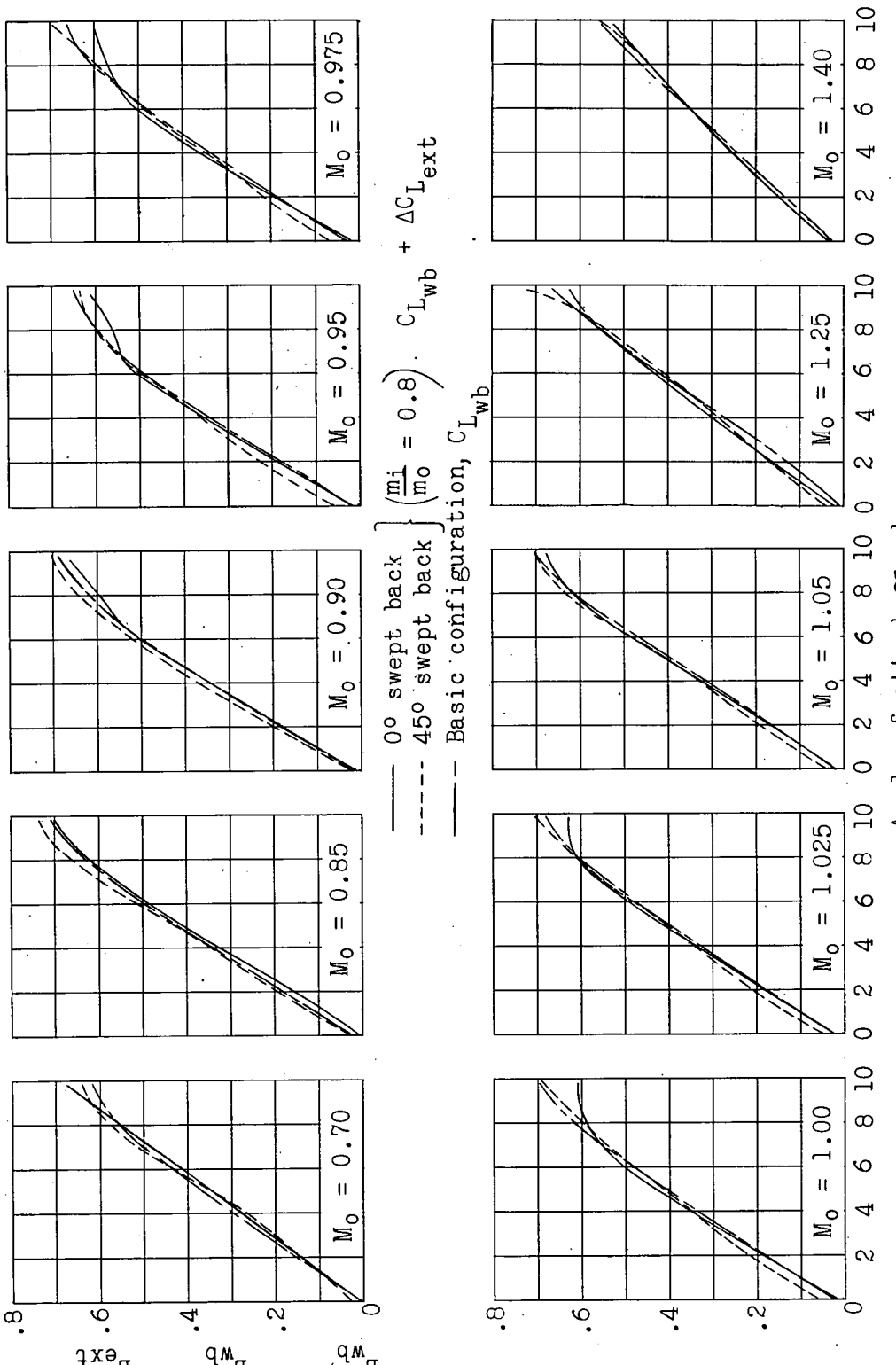

Figure 8.- Variation with angle of attack of lift coefficient of basic body and inlet configurations.

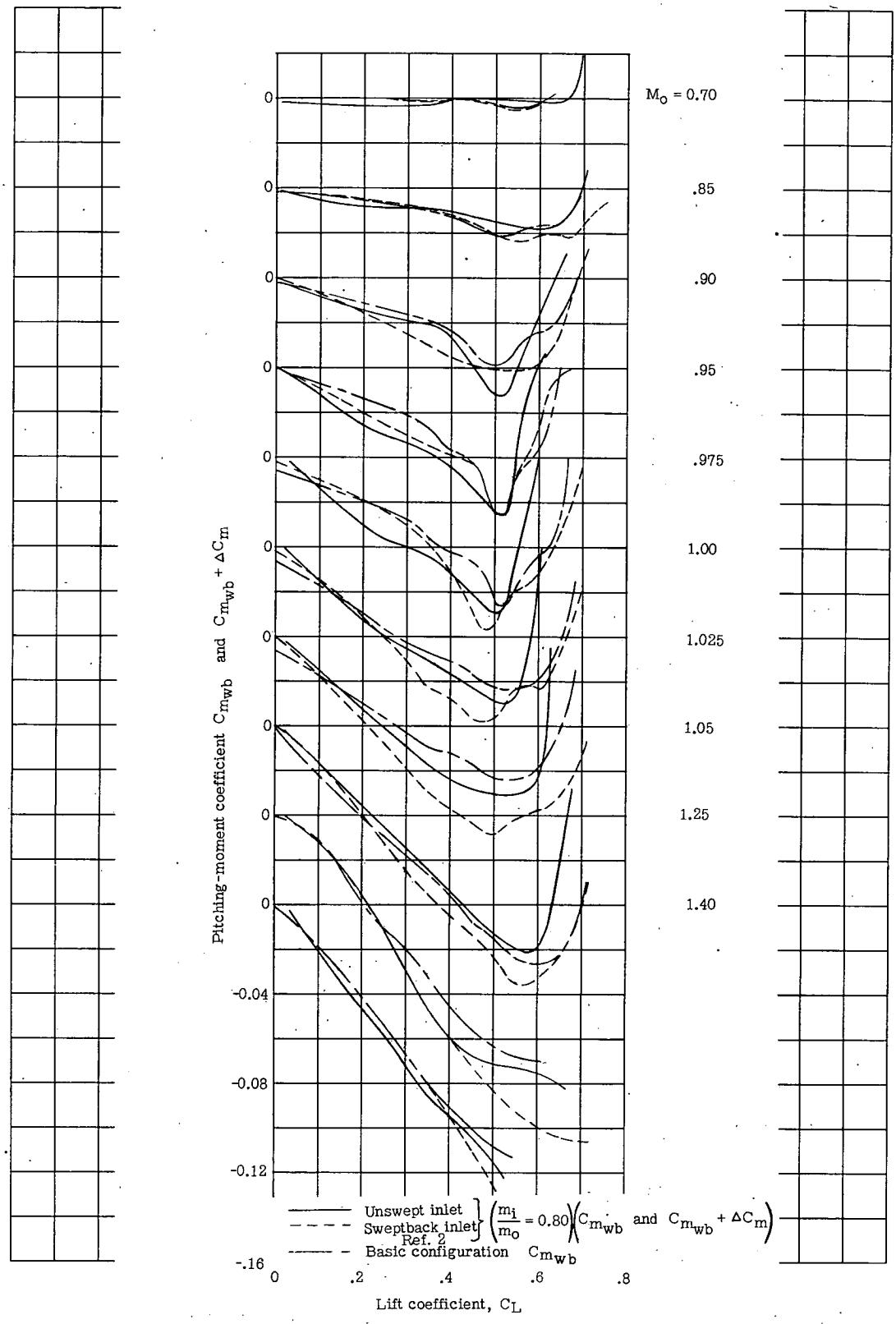

Figure 9.- Comparison of variation of pitching-moment coefficient with lift coefficient for basic model and two inlet configurations.

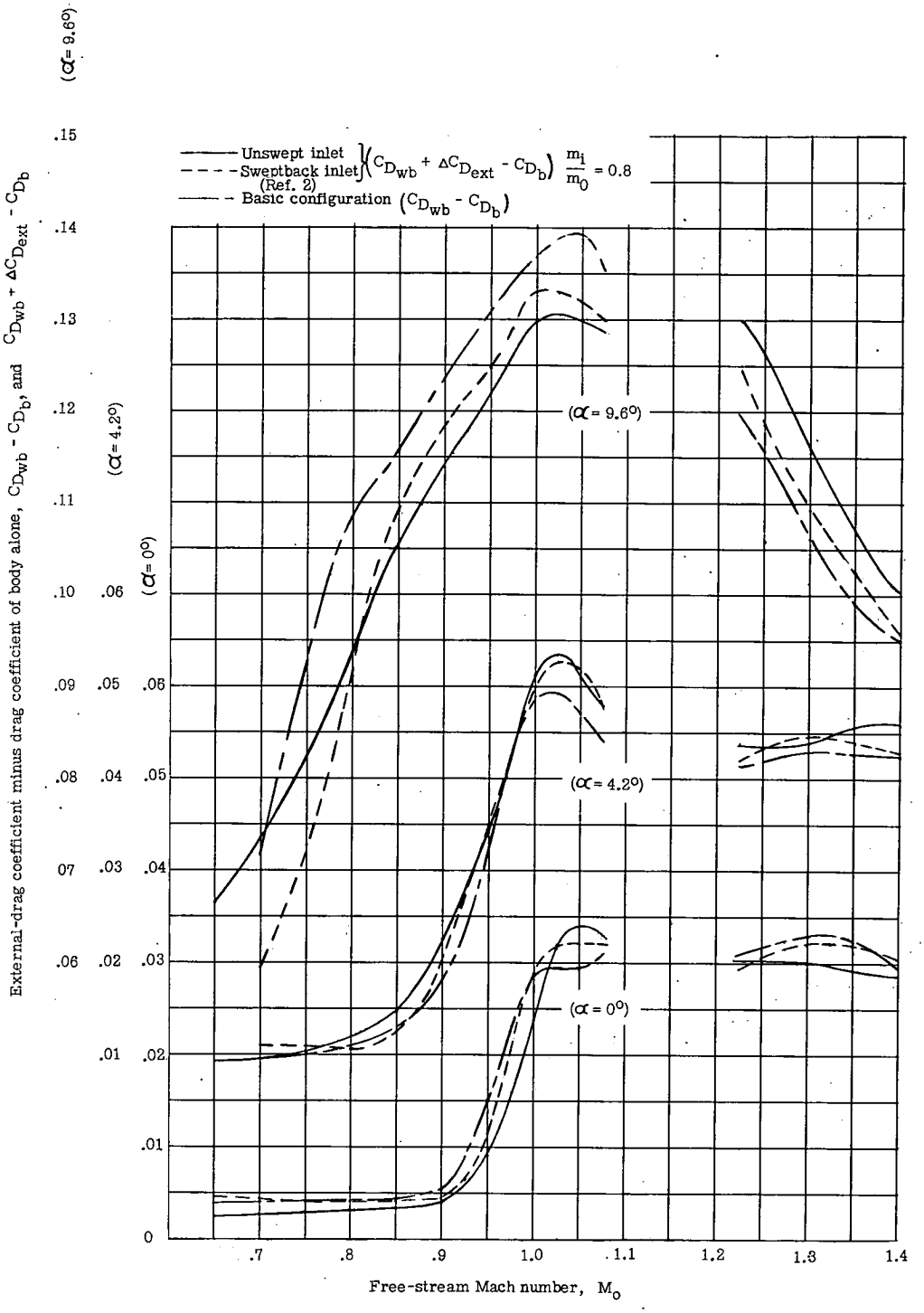

(a) Effect of Mach number.

Figure 10.- Effect of variation of Mach number, angle of attack, and mass-flow ratio on external-drag coefficient.

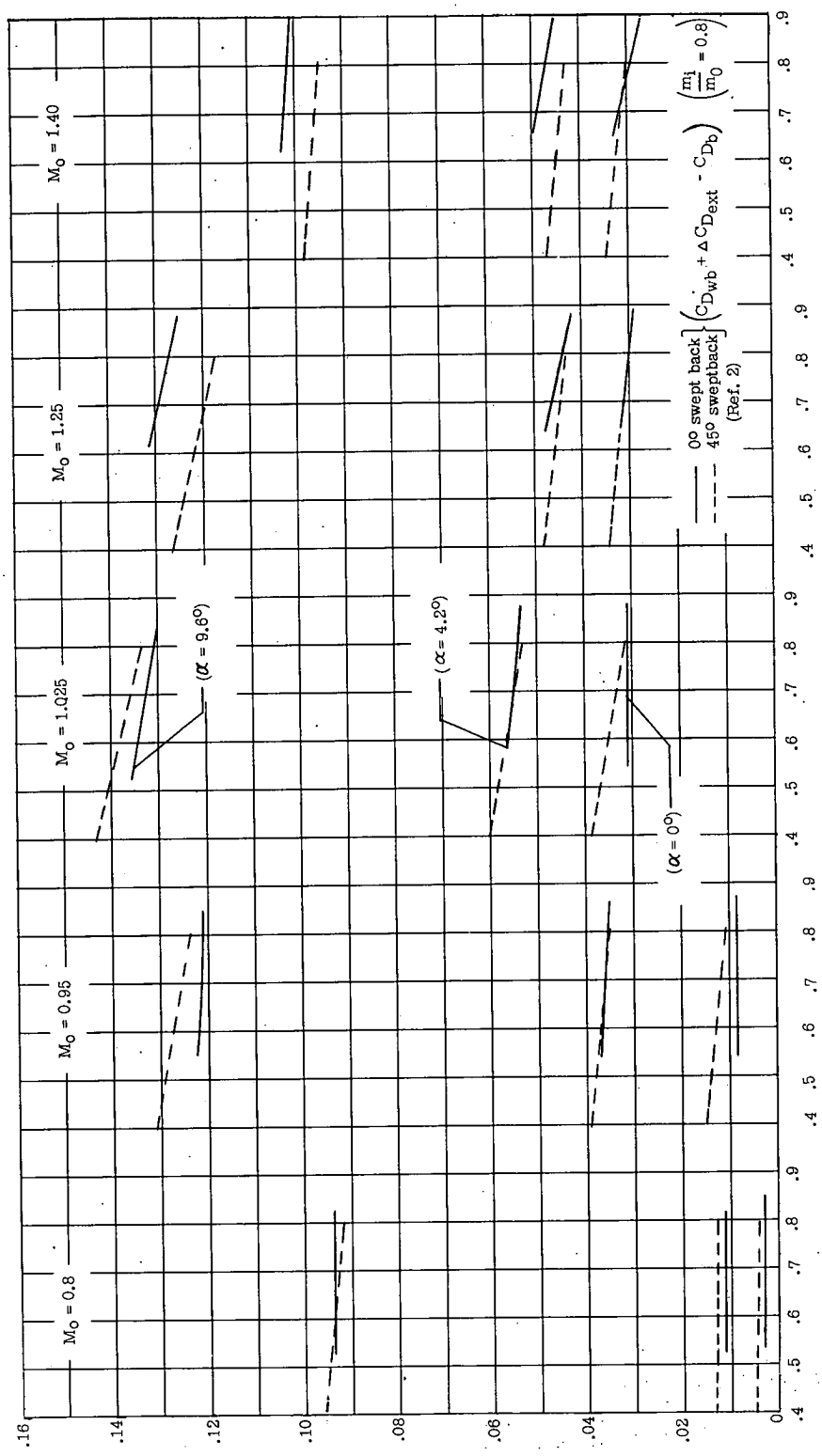

(b) Effect of mass-flow ratio and angle of attack.

Figure 10.- Concluded.

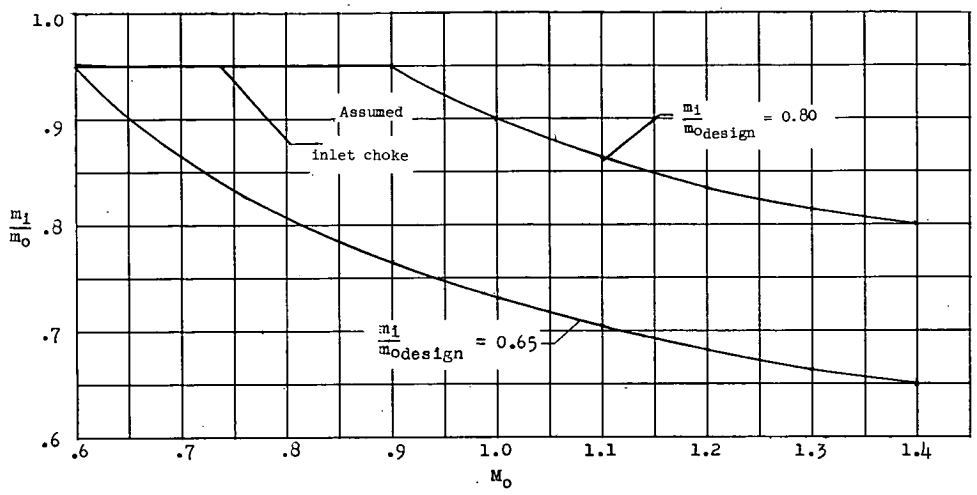

(a) Inlet mass-flow-ratio schedules.

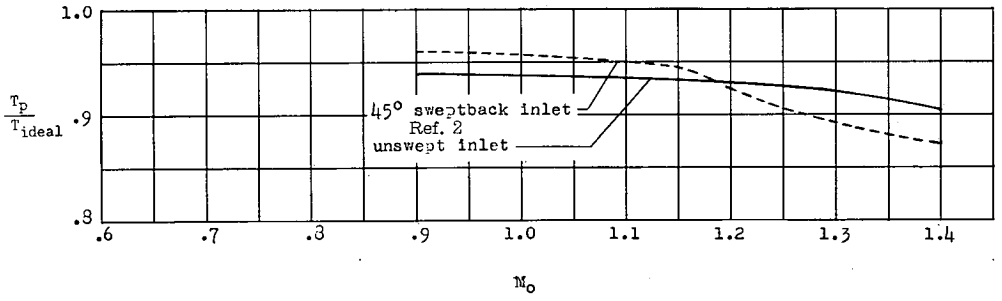

(b) Net thrust ratio for $\frac{m_i}{m_{o_{design}}} = 0.80$.

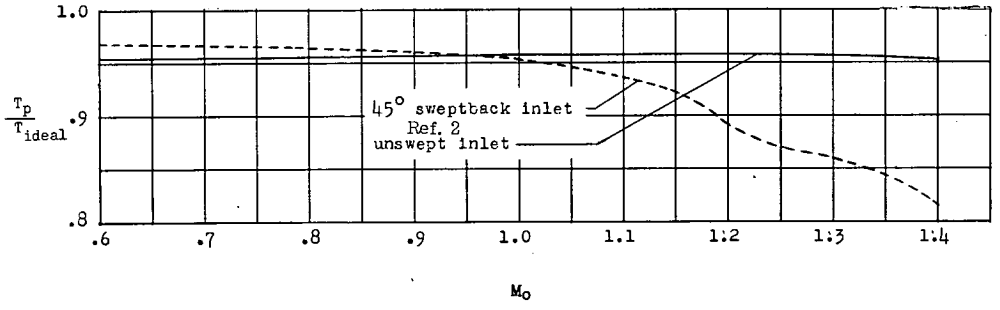

(c) Net thrust ratio for $\frac{m_i}{m_{o_{design}}} = 0.65$.

Figure 11.- Comparison of net engine thrust ratios for 45° sweptback inlet and for unswept inlet. $\alpha = 0^\circ$.

NACA - Langley Field, Va.